Am J Physiol Heart Circ Physiol 311: H384–H394, 2016.
First published June 24, 2016; doi:10.1152/ajpheart.00208.2016.

Hyperplasia, de novo lymphangiogenesis, and lymphatic regression in mice with tissue-specific, inducible overexpression of murine VEGF-D

Gabriela M. Lammoglia,[1]* Carolynn E. Van Zandt,[1]* Daniel X. Galvan,[1]* Jose L. Orozco,[2] Michael T. Dellinger,[3] and Joseph M. Rutkowski[1,2]

[1]*Division of Lymphatic Biology, Department of Medical Physiology, Texas A&M Health Science Center School of Medicine, College Station, Texas;* [2]*Touchstone Diabetes Center, Department of Internal Medicine, University of Texas Southwestern Medical Center, Dallas, Texas; and* [3]*Department of Surgery, University of Texas Southwestern Medical Center, Dallas, Texas*

Submitted 4 March 2016; accepted in final form 13 June 2016

Lammoglia GM, Van Zandt CE, Galvan DX, Orozco JL, Dellinger MT, Rutkowski JM. Hyperplasia, de novo lymphangiogenesis, and lymphatic regression in mice with tissue-specific, inducible overexpression of murine VEGF-D. *Am J Physiol Heart Circ Physiol* 311: H384–H394, 2016. First published June 24, 2016; doi:10.1152/ajpheart.00208.2016.—Lymphatic vessels modulate tissue fluid balance and inflammation and provide a conduit for endocrine and lipid transport. The growth of new lymphatic vessels in the adult, lymphangiogenesis, is predominantly mediated through vascular endothelial growth factor receptor-3 (VEGFR-3) signaling. We took advantage of the unique binding of murine VEGF-D specifically to VEGFR-3 and generated mice capable of inducible, tissue-specific expression of murine VEGF-D under a tightly-controlled tetracycline response element (TRE) promoter to stimulate adult tissue lymphangiogenesis. With doxycycline-activated expression, TRE-VEGF-D mouse crossed to mice with tissue-specific promoters for the lung [Clara cell secretory protein-reverse tetracycline transactivator (rtTA)] developed pulmonary lymphangiectasia. In the kidney, (kidney-specific protein-rtTA × TRE-VEGF-D) mice exhibited rapid lymphatic hyperplasia on induction of VEGF-D expression. Crossed with adipocyte-specific adiponectin-rtTA mice [Adipo-VEGF-D (VD)], chronic VEGF-D overexpression was capable of inducing de novo lymphangiogenesis in white adipose tissue and a massive expansion of brown adipose tissue lymphatics. VEGF-D expression in white adipose tissue also increased macrophage infiltration and tissue fibrosis in the tissue. Expression did not, however, measurably affect peripheral fluid transport, the blood vasculature, or basal metabolic parameters. On removal of the doxycycline stimulus, VEGF-D expression returned to normal, and the expanded adipose tissue lymphatics regressed in Adipo-VD mice. The inducible TRE-VEGF-D mouse thus provides a novel murine platform to study the adult mechanisms and therapies of an array of disease- and tissue-specific models of lymphangiogenesis.

VEGFR-3; lymphangiogenesis; adipose tissue; kidney; lymphangiectasia

NEW & NOTEWORTHY

A new mouse model of inducible murine VEGF-D expression drives lymphatic expansion. Lung, kidney, or brown adipose tissue (BAT) VEGF-D overexpression causes lymphatic hyperplasia and in white adipose tissue a de novo lymphatic network. New adipose lymphatics rapidly regress with basal VEGF receptor-3 signaling, providing a mechanistic model of adult lymphatic remodeling.

LYMPHATIC VESSELS ARE AN INTEGRAL part of the body's circulatory system that are gaining an increased appreciation due to their wide-ranging roles in tissue homeostasis and disease. Interstitial fluid, macromolecules, and immune cells enter lymphatics in the periphery and are transported to draining lymph nodes. In this capacity, lymphatics play a critical role in modulating tissue fluid balance and inflammation and provide a conduit for endocrine and lipid transport (27, 34, 37). Changes in lymphatic vessel architecture, integrity, and function have been described and implicated in congenital and acquired conditions of aging, inflammatory disease, lymphedema, and lipedema (12, 13, 23, 24, 50). Lymphangiogenesis, the growth of new lymphatic vessels, has been proposed as a potential therapy to many of these conditions, but is also a characteristic pathological response to inflammation, tumor progression, and chronic lymphatic-related diseases, such as lymphangioleiomyomatosis (35, 53). Models to study adult lymphangiogenesis and its effects are thus useful to the growing field of lymphatic research.

The most well-characterized mechanism of lymphatic endothelial cell (LECs) proliferation, and hence lymphangiogenesis, is through vascular endothelial growth factor receptor-3 (VEGFR-3) phosphorylation on binding its primary ligands, VEGF-C and VEGF-D (47, 57). VEGF-C and VEGF-D expression, through direct treatment, adenoviral expression, or transgenic overexpression, demonstrate the ability to induce lymphangiogenesis critically through VEGFR-3 activation, but also potentially induces blood vessel growth and permeability through binding to VEGFR-2 (11, 32, 40, 47). Interestingly and importantly, murine VEGF-D binds only to VEGFR-3, affording an opportunity to specifically target a lymphatic- and lymphangiogenesis-specific pathway in the adult mouse (4, 5).

Here we describe the generation and characterization of a novel mouse model with doxycline-inducible expression of full-length murine VEGF-D, the tetracycline response element (TRE) VEGF-D (TRE-VD) mouse. Crossed with mice carrying a transgene for cell- or tissue-specific promoter reverse tetracycline transactivator (rtTA), VEGF-D expression can be locally induced. We demonstrate that murine VEGF-D overexpression specifically induces lymphangiogenesis in the tissues of mice carrying rtTA promoter transgenes specific to the lung, kidney, and adipose tissue, and that lymphatic expansion regresses once VEGF-D overexpression ends. The TRE-VD mouse thus provides an excellent novel platform for expanded studies of lymphatic mechanisms in adult disease.

* G. M. Lammoglia, C. E. Van Zandt, and D. X. Galvan contributed equally to this work.

Address for reprint requests and other correspondence: J. M. Rutkowski, Div. of Lymphatic Biology, Dept. of Medical Physiology, Texas A&M Health Science Center School of Medicine, 345 Reynolds Bldg., College Station, TX 77843-1114 (e-mail: rutkowski@tamu.edu).

MATERIALS AND METHODS

Animals. New TRE promoter VEGF-D mice were generated. Briefly, the full-length murine VEGF-D coding sequence (NM_010216) was cloned from murine inguinal adipose tissue (including the inguinal lymph node) cDNA preceded by a Kozac sequence of 5′-GCCGCCACC-3′ to enhance translation. The DNA was inserted into the pTRE-Tight (Clontech) vector, having been cloned with restriction enzyme sites for *Nhe*I and *Xba*I and the rabbit β-globin 3′-UTR placed at the 3′ end. Linearized DNA was injected into C57Bl/6N embryos by the Transgenic Technology Center at UT Southwestern. Genotyping to identify positive founder lines was performed with primers that bridged the TRE promoter and inserted mVEGF-D gene: forward, GCTCGTTTAGTGAACCGTCAG, and reverse, TGCTCGGATCTGTTGTTCAG, respectively.

Positive pTRE-Tight-VEGF-D transgenic lines were mated to homozygosity with the previously described adiponectin-promoter (*AdipoQ*) advanced rtTA mice for adipose-specific expression (46, 51). pTRE-Tight-VEGF-D (TRE-VD) mice were also crossed with kidney specific protein (KSP)-rtTA (31) (from the George M. O'Brien Kidney Research Core at UT Southwestern) and Clara cell secretory protein (CCSP)-rtTA (6) (from The Jackson Laboratory, Bar Harbor, ME) mouse lines to generate mice with doxycycline (dox)-inducible VEGF-D expression in the kidney and lung, respectively. All were continuously backcrossed to C57Bl/6J for at minimum three generations.

For initial founder line characterizations and breeding, both males and females were utilized (3 mice total per group). All experiments were performed with male-only littermate mice, all of which were hemizygous for the TRE-VEGF-D transgene, but were either wild type or hemizygous for their respective rtTA. Four to five mice per genotype per group were utilized in all tests. Mice were housed in pathogen-free conditions with 12:12-h light-dark cycles and ad libitum access to water and food. Experimental dox-containing chow diet (Research Diets) of either 600 or 200 mg/kg (or 50 and 100 mg/l water) was supplied to all mice in an experiment, as indicated, to eliminate any dox artifacts, such that all mice were equally dosed. Thus, in all studies, all mice carry equal copies of the TRE-VD transgene and receive dox; the presence or absence of the rtTA promoter transgene provided our "control" and "test" groups, respectively. All animal study protocols were approved by the Institutional Animal Care and Use Committee at UT Southwestern and/or Texas A&M University.

Body composition analysis. Body composition of mice (4 −rtTA, 6 +rtTA) was measured by NMR on a Bruker LF50 BCA-Analyzer before euthanization. Composition is reported as percentage of total mass lean, fat, and fluid.

Tissue, protein, and RNA preparation. Following exsanguination under isofluorane, tissues were harvested and either immediately fixed in 10% buffered formalin or flash frozen in liquid N_2 for protein and RNA extractions. Cells and proteins were extracted by homogenization in TNET buffer (50 mM Tris, 150 mM NaCl, 1 mM EDTA, 1% Triton X-100, pH 8.0) with protease and phosphatase inhibitors added (Roche). For adipose depots, detergent-free buffer was used, the samples spun to remove excess lipid, 10% Triton X-100 added (for a final 1%), and pellet rehomogenized. All proteins were normalized to 1 mg/ml in TNET. For gel electrophoresis, samples were heated for 5 min at 95°C in 5× Laemmli buffer containing 100 mM dithiothreitol. RNAs were extracted using a Qiagen RNeasy Mini Kit, according to the manufacturer's instructions (Qiagen, Germantown, MD). Reverse transcription of 1 μg RNA was done according to the iScript cDNA Synthesis kit instructions (Bio-Rad Laboratories, Hercules, CA).

Histology and immunofluorescence. Following 24 h in 10% buffered formalin, tissues were rinsed in water and stored in 50% ethanol until paraffin embedding. Three-micrometer-thick sections were cut from all tissues. Adipose depots were sectioned to maximize area (and to include the lymph node, in the case of inguinal adipose), and kidneys and lungs were sectioned sagittally. Whole mount tissues were submersion fixed in 10% buffered formalin for 2 h, followed by multiple hour-long rinses in 0.1% Triton X-100 in PBS.

Tissue sections were stained by Masson's trichrome method for visualizing adipose tissue and matrix density. For immunofluorescence, sections were deparaffinized, rehydrated, and subjected to 10-min citrate buffer boiling (Vector Labs, Burlington, CA) antigen retrieval when necessary. Tissues were labeled with primary antibodies to murine VEGF-D (goat polyclonal; R&D Systems, Minneapolis, MN), lymphatic vessel endothelial hyaluronan receptor-1 (LYVE-1) (goat polyclonal; R&D Systems), podoplanin (goat polyclonal; R&D Systems), Prox-1 (rabbit polyclonal; AngioBio, San Diego, CA), CD31 (rabbit polyclonal; Abcam, Cambridge, MA), endomucin (rat polyclonal; Santa Cruz Biotechnology, Dallas, TX), and Ki67 (rabbit polyclonal; Abcam). Secondary detection was by Alexafluor 488- or 594-labeled donkey or chicken antibodies (Life Technologies, Carlsbad, CA). Immunofluorescence was imaged using a Zeiss AxioObserver fluorescence microscopy system and MRc camera or a Nikon Eclipse E600 microscope, and images were captured using NIS-Elements imaging software.

Image quantification. Double-blinded image quantitation of immunofluorescence images was performed in ImageJ software by measuring the area of each image above a set color threshold on the green (LYVE-1) and red (endomucin) channels of the image to represent vessel area, not capillary density. For adipose tissue, four to five images were captured at ×10 from each mouse sample (4 −rtTA, 5 +rtTA; for dox withdrawal study subcutaneous adipose 4 −rtTA, 4 +rtTA and brown adipose $n = 8$ each) with care taken to avoid tissue defects, edges, and the inguinal lymph node (in subcutaneous adipose). For kidney (KSP-rtTA), one image was captured in the sinus from each mouse, and four ×10 images were taken at the corticomedullary junction (4 −rtTA, 3 +rtTA). Area values were normalized to the average of the −rtTA group and presented as relative area of positive label.

Oral glucose tolerance test and lipid clearance. An oral load or 1.4 mol/l glucose solution at 10 μl/g or Intralipid at 10 μl/g was given following a 3-h fast. Blood samples were collected from the tail tip at the times indicated in the experiments. Glucose and serum triglycerides were measured by Sigma Diagnostics Glucose reagent and Infinity reagent (Thermo) spectrophotometric assay, respectively. Tests were performed 10 days apart on the same group of four −rtTA and six +rtTA mice.

Quantitative real-time RT-PCR. Power SYBER Green PCR Master Mix (Applied Biosystems) was used with adipose, kidney, and lung cDNA on an Applied Biosystems 7900 quantitative PCR machine. For founder characterizations, three mice of each were tested, and *Rps18* was used as an endogenous control after 10 days of 600 mg/kg dox induction. Comprehensive analyses in adipose tissues utilized four to five mice per genotype and *Ubc* as a universal control. Primer sequences are listed in Table 1.

Lymph node fluorescence uptake. Fifty-microliter intradermal injections of 2 mg/ml Texas red dextran (70 kDa; Invitrogen) were made into each hind footpad. Mice (4 −rtTA, 5 +rtTA) were euthanized 45 min later by exsanguination under isofluorane, and the popliteal and inguinal lymph nodes were collected. Nodes were homogenized in 250 μl PBS, and the fluorescence density at 564 nm was measured on an Optima fluorescence plate reader. Protein concentration of node homogenates was measured by BCA. Measured fluorescence values were normalized to protein concentration and expressed as fluorescence units per milligram protein.

Evans blue injection. Seven mice (3 −rtTA, 4 +rtTA) were injected intravenously with a 0.5% Evans blue dye solution (in sterile saline; Sigma) at 100 μl/30 g body wt to assess Evan's blue-bound protein flux from blood capillaries. After 30 min, mice were euthanized by exsanguination under isofluorane, and tissues were removed and weighed. Tissues were dried in a vacuum oven then extracted in 500 μl formamide overnight. Evans blue absorbance was measured at

Table 1. *Primer sequences utilized for quantitative RT-PCR analysis of murine subcutaneous adipose tissue*

Target	Forward	Reverse
AdipoQ	GGAGATGCAGGTCTTCTT	CGAATGGGTACATTGGGAAC
Cd11c	CTGGATAGCCTTTCTTCTGCTG	GCACACTGTGTCCGAACTC
Cd3e	GATGCGGTGGAACACTTTCT	ACTGTCCTCGACTTCCGAGA
Col1a1	GCCAAGAAGACATCCCTGAA	GTTTCCACGTCTCACCATTG
Col3a1	ACAGCTGGTGAACCTGGAAG	ACCAGGAGATCCATCTCGAC
Col4a1	ACAAAAGGGTGATGCTGGAG	CCTTTGTACCGTTGCATCCT
Col6a1	GATGAGGGTGAAGTGGGAGA	CAGCACGAAGAGGATGTCAA
F4/80	CTGTAACCGGATGGCAAACT	CTGTACCCACATGGCTGATG
Fn/Adgre1	ACAAGGTTCGGGAAGAGGTT	CCGTGTAAGGGTCAAAGCAT
Il-6	GAGGATACCACTCCCAACAGACC	AAGTGCATCATCGTTGTTCATA
Lyve1	CTGACAAGCAGTTTCAGGCTTGGT	TTCAGCCCACACTCCGCTATACAT
Resistin/Fizz3	TCGTGGGACATTCGTGAAGA	CGGGCTGCTGTCCAGTCTA
Rps18	CATGCAGAACCCACGACAGTA	CCTCACGCAGCTTGTTGTCTA
Tnf	GAGAAAGTCAACCTCCTCTCTG	GAAGACTCCTCCCAGGTATATG
Ubc	GCCCAGTGTTACCACCAAGAAG	GCTCTTTTTAGATACTGTGGTGAGGAA
Vegfa	GGAGATCCTTCGAGGAGCACTT	GGCGATTTAGCAGCAGATATAAGAA
Vegfb	TGACATCATCCATCCCACTC	CCTTGGCAATGGAGGAAG
Vegfc	GGTCCACAGACATCATGGAA	CAGTGTCAGGCAGCTAACAAG
Vegfd/Figf	AAATCGCGCACTCTGAGGA	TGGCAAGACTTTTGAGCTTCAA
Vegfr2/Flk1	GCCCTGCTGTGGTCTCACTAC	CAAAGCATTGCCCATTCGAT
Vegfr3/Flt4	ATCAGAAGATCGGGCGCTGTTGTA	TGTGTCATGTCCGCCCTTCAGTTA

Common names and variant names are provided. All sequences were verified through National Center for Biotechnology Information Primer-BLAST, and single products confirmed with a dissociation step postamplification.

620 nm and normalized to wet tissue mass, thus expressed as absorbance units per milligram tissue.

Statistical analysis and data presentation. In all studies, all mice carry equal copies of the TRE-VD transgene. The lack or presence of the cell-specific promoter rtTA designates the control vs. mutant group, respectively. Four to five mice per group were used in each experiment; founder identification RNA expressions used two to three per group. In each experiment, statistical analyses were *t*-test comparisons between the control vs. mutant group using GraphPad Prism software. Asterisks denote significant differences (*$P < 0.05$, **$P < 0.01$, and *** $P < 0.01$). All data are presented as means ± SD.

RESULTS

Generation and characterization of a new inducible VEGF-D expressing mouse. To inducibly express murine VEGF-D protein in mammalian cells, the coding sequence for full-length VEGF-D_{358} (*Figf.1*; NM_010216) was cloned from murine adipose tissue cDNA and inserted into a TRE vector containing a minimal CMV promoter sequence (pTRE-Tight). This TRE-*Figf.1* expression vector was transfected into 293T cells with or without expression of the rtTA. Cell lysates demonstrated marked VEGF-D protein expression in the presence of the full Tet-On genetic system and 1 μg/ml dox in the media (Fig. 1*A*). This vector was linearized for pronuclear injection of murine embryos, and multiple founder lines were established. These were crossed with mice carrying various promoter-driven rtTAs, including CCSP(*Scgb1a1*)-rtTA, KSP(*Cdh16*)-rtTA, and adiponectin(*AdipoQ*)-rtTA mouse lines (Fig. 1*B*). To test for functionality and gene expression "leakiness" of the TRE-VEGF-D_{358} (TRE-VD) transgene, mice were crossed with *AdipoQ*-rtTA to homozygosity. Two lines demonstrated a

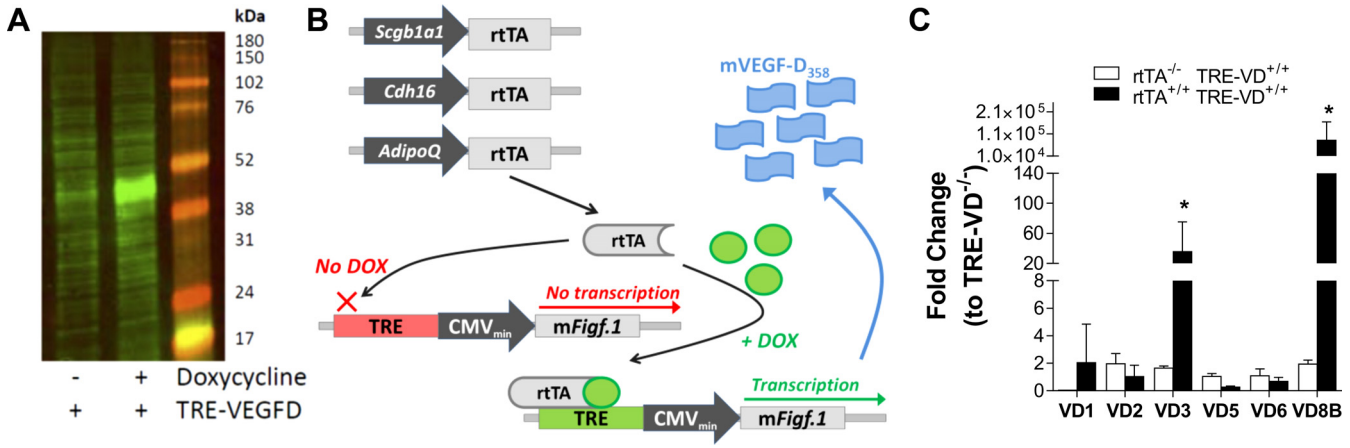

Fig. 1. Generation and validation of the TRE-VEGF-D mouse. *A*: transfection of 293T cells stably expressing rtTA demonstrate significant expression of murine VEGF-D protein only on exposure to doxycycline (dox) assessed by immunoblot. *B*: transgenic mouse strategy and demonstration of the "Tet-on" dox system for crossing the TRE-VEGF-D to mice for cell-specific expression using promoters in the lung (*Scgb1a1*; CCSP), kidney (*Cdh16*; KSP), and adipose (*AdipoQ*; adiponectin) tissues. The TRE-Tight gene construct (m*Figf.1*) used to express full-length murine VEGF-D_{158} is shown. *C*: VEGF-D gene expression levels in *AdipoQ-rtTA*$^{+/+}$ × *TRE-VD*$^{+/+}$ mice in subcutaneous adipose tissue after 7–10 days of 600 mg/kg dox chow diet. The VD3 line was selected and maintained for all experiments. Values are means ± SD. *$P < 0.05$.

significant induction of murine VEGF-D RNA expression when placed on a 600 mg/kg dox-containing chow for 10 days. Live VD8B was deemed too high of an expresser and bred poorly. Line VD3 on the pTRE-Tight promoter (Fig. 1*C*) was selected due to tight regulation and a physiologically-relevant (×20) elevation (53).

VEGF-D overexpression in the lung induces pulmonary lymphangiectasia. As a previous effort to utilize a lymphangiogenic growth factor, VEGF-C, in the lung had recently demonstrated feasibility and induced extensive lymphatic hyperplasia without lethality (54), we tested whether the TRE-VD mouse would also exhibit adult bronchiolar lymphangiectasia. After 1 mo on dox chow, there was no visible change in mouse behavior and, following euthanization, no pleural fluid. Lung lysate from *CCSP-rtTA*$^{+/-}$ × *TRE-VD*$^{+/-}$ mice did, however, demonstrate significantly elevated VEGF-D mRNA (Fig. 2*A*). VEGF-D protein expression by immunofluorescence was tightly limited to epithelial club cells identified by punctate VEGF-D labeling in the epithelium (Fig. 2*B*). These levels were sufficient to induce lymphangiectasia in the existing bronchiolar lymphatic vessels (Fig. 2*C*) comparable to the response to VEGF-C induction (54).

Renal lymphangiectasia resulting from VEGF-D expression in the kidney. Lymphangiogenesis occurs in the kidney during inflammatory events, but its impact is yet unknown (55). To test whether induction of VEGF-D in a quiescent kidney would induce lymphatic expansion, KSP-rtTA mice were crossed with the TRE-VD mouse. After dox diet for 1 wk, elevated VEGF-D RNA was measured in the renal cortex (Fig. 3*A*), and VEGF-D protein was highly expressed specifically in renal tubular epithelial cells (Fig. 3*B*). A massive expansion of the large collecting lymphatic vessels at the renal cortex was discovered in *KSP-rtTA*$^{+/-}$ × *TRE-VD*$^{+/-}$ mice (Fig. 3*C*). Image quantification of LYVE-1+ area confirmed this significant lymphangiectasia (Fig. 3*D*). While an increase in lymphatics in the cortex was seen in some mice at this time, the change in the collecting lymphatics was the most striking pathological change in the lymphatic vasculature (Fig. 3*E*).

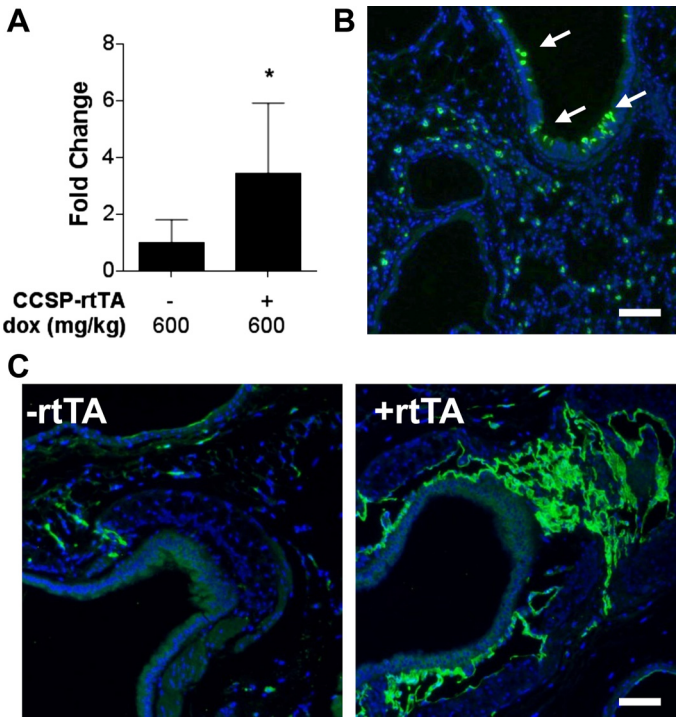

Fig. 2. Pulmonary lymphangiectasia resulting from VEGF-D overexpression in the lung. *A*: VEGF-D gene expression in the lung of *CCSP-rtTA* × *TRE-VD* mice. Values are means ± SD. *$P < 0.05$. *B*: VEGF-D protein expressed (green) in respiratory club cells by immunofluorescence (DAPI, blue) (arrows highlight a few location). *C*: massive lymphatic hyperplasia (LYVE-1, green) of the bronchiolar lymphatics (DAPI, blue) in CCSP-VD mice. All mice carry the TRE-VD transgene but are + or − for rtTA. All scale bars = 100 μm.

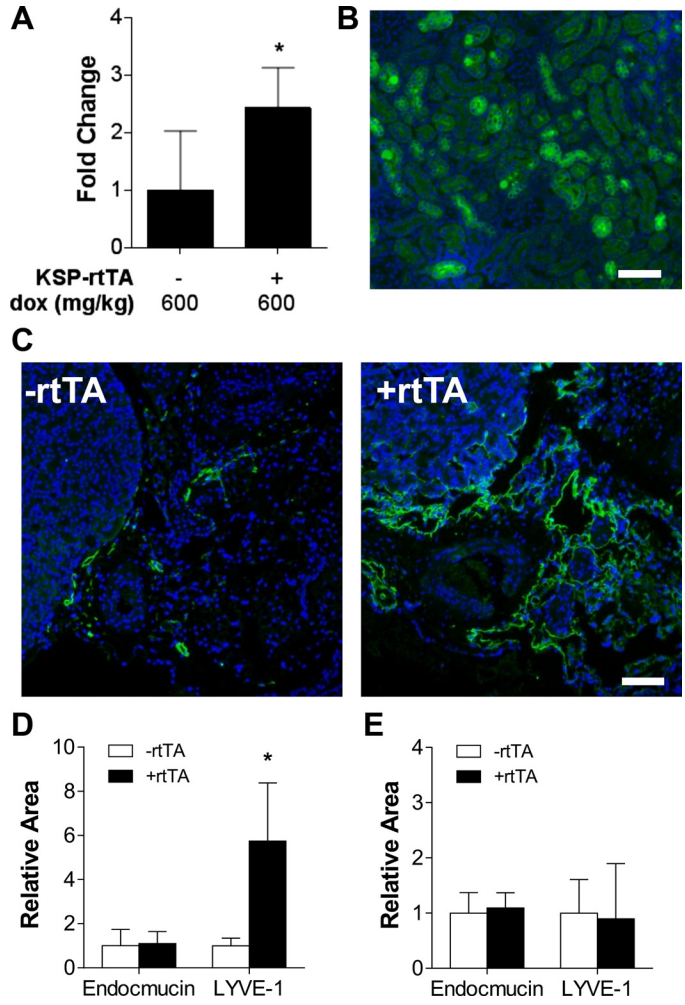

Fig. 3. Rapid renal lymphangiectasia upon induction of kidney-specific VEGF-D overexpression. *A*: VEGF-D gene expression in the renal cortex of *KSP-rtTA* × *TRE-VD* mice. *B*: VEGF-D protein expressed in tubular epithelial cells by immunofluorescence (green; DAPI, blue). *C*: massive lymphatic hyperplasia (LYVE-1, green) of the renal collecting lymphatics that run along the renal artery and vein (DAPI, blue). All scale bars = 100 μm. *D*: quantified endomucin+ and LYVE-1+ areas (normalized to −rtTA) on images of the renal sinus from 4 mice demonstrate lymphatic expansion. *E*: endomucin+ and LYVE-1+ areas in the renal cortex identify no changes in the cortical vasculature. All mice carry the TRE-VD transgene but are + or − for rtTA. Values are means ± SD; $n = 4$ −rtTA and 3 +rtTA mice. *$P < 0.05$.

Inducible VEGF-D expression drives de novo lymphangiogenesis in adipose tissues. Adipose tissue circulation and vascular adaptation to changes in adipose physiology are critical in regulating systemic metabolism (37, 46). Past strategies have targeted the blood vasculature of adipose tissue, but, with TRE-VD mouse, we sought to specifically target lymphatic endothelium. *AdipoQ-rtTA*$^{+/-}$ × *TRE-VD*$^{+/-}$ mice (Adipo-

VD) were supplied a range of dox doses, from 50 to 600 mg/kg chow or water (equivalent to 50–600 mg/l in water), for 10 days, and VEGFD RNA expression was measured in the subcutaneous white adipose inguinal depot [subcutaneous adipose tissue (SQAT)] or the interscapular brown adipose (BAT) depot. Dox induced a dose-responsive increase in VEGFD RNA levels in both depots, with a more significant effect in BAT (Fig. 4*A*). Removal of 600 mg/kg dox chow from mice for 2 mo resulted in a normalization of VEGF-D expression (Fig. 4*A*). The SQAT depot was mostly a lymphatic by LYVE-1 immunofluorescence (Fig. 4*B*), but 600 mg/kg dox chow for 2 mo (no cellular response was seen at 10 days) drove marked de novo lymphangiogenesis in adipose tissue with LYVE-1$^+$ structures throughout the tissue (and not only adjacent to the lymph node). Quantitation of vessel density demonstrated the significant increase in lymphatic endothelium with no change in blood endothelium (Fig. 4*C*). The effect of VEGF-D induced lymphatic hyperplasia was even more pronounced in the highly-vascularized BAT depot (Fig. 4, *D* and *E*). Expanded lymphatics were also podoplanin+ and Prox-1+ structures (Fig. 4*F*). Whole-mount immunofluorescence in BAT (Fig. 4*G*) identified the increase in LYVE-1+ labeling to be new hypertrophic lymphatic vessel structures. Despite inducing significant VEGF-D RNA, lower doses of dox or times less than 1 mo failed to elicit de novo lymphangiogenesis in either adipose tissue depot (data not shown). Confirming the VEGFR-3 specificity, no new lymphatic vessels were found in the adipose tissue of the previously described *AdipoQ-rtTA* × *TRE-VEGF-A* (46) (Fig. 4*H*) The Adipo-VD mouse thus demonstrated that controlled, inducible adult adipose tissue lymphangiogenesis was possible.

Effects of increased VEGF-D expression in adipose tissues beyond lymphangiogenesis. While VEGF-D overexpression elicits clear lymphangiogenesis in adipose tissue depots, VEGF-D also serves as a macrophage chemoattractant (20) in adipose tissue, potentially resulting in adipose tissue inflammation and the metabolic syndrome (39). Real-time RT-PCR analysis of genes related to the VEGF family and its receptors demonstrated only a significant increase in VEGF-D expression in SQAT RNA (Fig. 5*A*). LYVE-1, as marker of LECs was also increased. Expression of adipose tissue macrophage markers *F4/80* and *CD11c* were also significantly increased. Supporting immunofluorescence identified very few Mac-2+ adipose tissue macrophages in control SQAT, while large numbers were labeled in positive Adipo-VD mouse tissue (Fig. 5*B*). While Mac-2+ cells were often nearby new LYVE-1+ structures, the labels did not overlap. Commiserate with increasing immune cell numbers, gene expression of white adipocyte markers adiponectin and resistin was significantly reduced (Fig. 5*C*). Increased levels of IL-6, fibrillary collagens, and fibrin were not statistically elevated, but matched the variability and overall increase in adipose tissue fibrosis visualized by trichrome staining (Fig. 5*D*). Macrophage density, along with fibrosis, was interrelated in each mouse tissue examined (Fig. 5*E*). The systemic implications of adipose tissue inflammation and VEGF-D expression were then tested.

Systemic effects of adipose tissue VEGF-D expression. VEGFR-3 signaling affects vascular function, and changes in adipose tissue physiology result in systemic changes in metabolism. Lymphatic hyperplasia and VEGFR-3 signaling can result in poorly functioning lymphatic vessels and increased vascular permeability (9, 15, 18).

In the Adipo-VD mouse, no significant reduction or enhancement was measured in the amount of 70-kDa fluorescent dextran, a size that partitions to lymphatics, that was transported from the mouse footpad, through the popliteal lymph node, and on to the inguinal lymph node (Fig. 6*A*). Intravenous Evans blue dye injections were used to measure systemic Evans blue-bound protein flux in a range of adipose and nonadipose tissues. No differences were measured in the amount in Evans blue extravasation in any tissue with VEGF-D expression (Fig. 5*B*). Similarly, and unlike specific VEGF-A overexpression in adipose tissue (46), no fluid accumulation was measured by NMR body composition analysis with heightened VEGF-D (Fig. 6*C*). Adipo-VD was well-tolerated: no Adipo-VD mice died, despite being supplied 600 mg/kg dox chow for up to 4 mo.

Body composition measures revealed no change in adiposity (Fig. 5*C*), important for assessing basal metabolic changes in Adipo-VD mice. No change in body weight was measured in Adipo-VD mice, even after nearly 3 mo of VEGF-D induction in adipose tissue (Fig. 6*D*). Despite the marked adipose tissue macrophage infiltration that has demonstrated the potential to impact systemic glucose clearance (1, 20, 33), no significant differences were measured in glucose levels in Adipo-VD mice during oral glucose challenge (Fig. 6*E*). Similarly, fasted oral triglyceride clearance was not significantly impacted (Fig. 6*F*). Thus we did not measure any transport or metabolic changes under the otherwise homeostatic condition of standard chow feeding with adipose tissue VEGF-D overexpression and lymphangiogenesis.

Basal VEGF-D levels permit lymphatic regression in SQAT. In mouse models wherein lymphangiogenesis was induced through transgenic or inflammatory means, the ability of lymphatic hyperplasia to resolve or new vessels to regress has varied from next to nothing to nearly complete (7, 10, 28, 54). Adipo-VD mice were provided 600 mg/kg for 2 mo, ample to drive the previously described lymphatic hyperplasia, then returned to standard chow diet for 2 mo. Immunofluorescence labeling identified few remaining LYVE-1+ structures in SQAT (Fig. 7*A*), with structures only made up of a few LECs, not uncharacteristic of native tissue. Image quantitation confirmed a reduction in LYVE-1+ area (Fig. 7*B*). Tissue sections from some mice revealed these LYVE-1+ cells to be surrounded by, colocalizing with, or integrating with Mac2+ macrophages and newly formed adipose tissue crown-like structures (Fig. 7*C*). These cells were also podoplanin+ (Fig. 7*D*), confirming that they were likely remnants of the de novo lymphatics induced in white adipose tissue. In interscapular BAT, many large hyperplastic lymphatic structures remained (Fig. 7*E*). Regression varied highly from mouse-to-mouse (Fig. 7*F*). BAT thus exhibits a more pronounced, and more prolonged, lymphatic hyperplasia following a period of VEGF-D induction.

Conclusons. We have generated and characterized a novel mouse model of inducible murine VEGF-D expression to target VEGFR-3 signaling on adult lymphatic vasculature to promote lymphangiogenesis. We took advantage of the unique signaling of murine VEGF-D specific to VEGFR-3, which is largely limited to LECs in the adult mouse (5), coupled with a dox-inducible "Tet-On" system of cell-specific promoter-

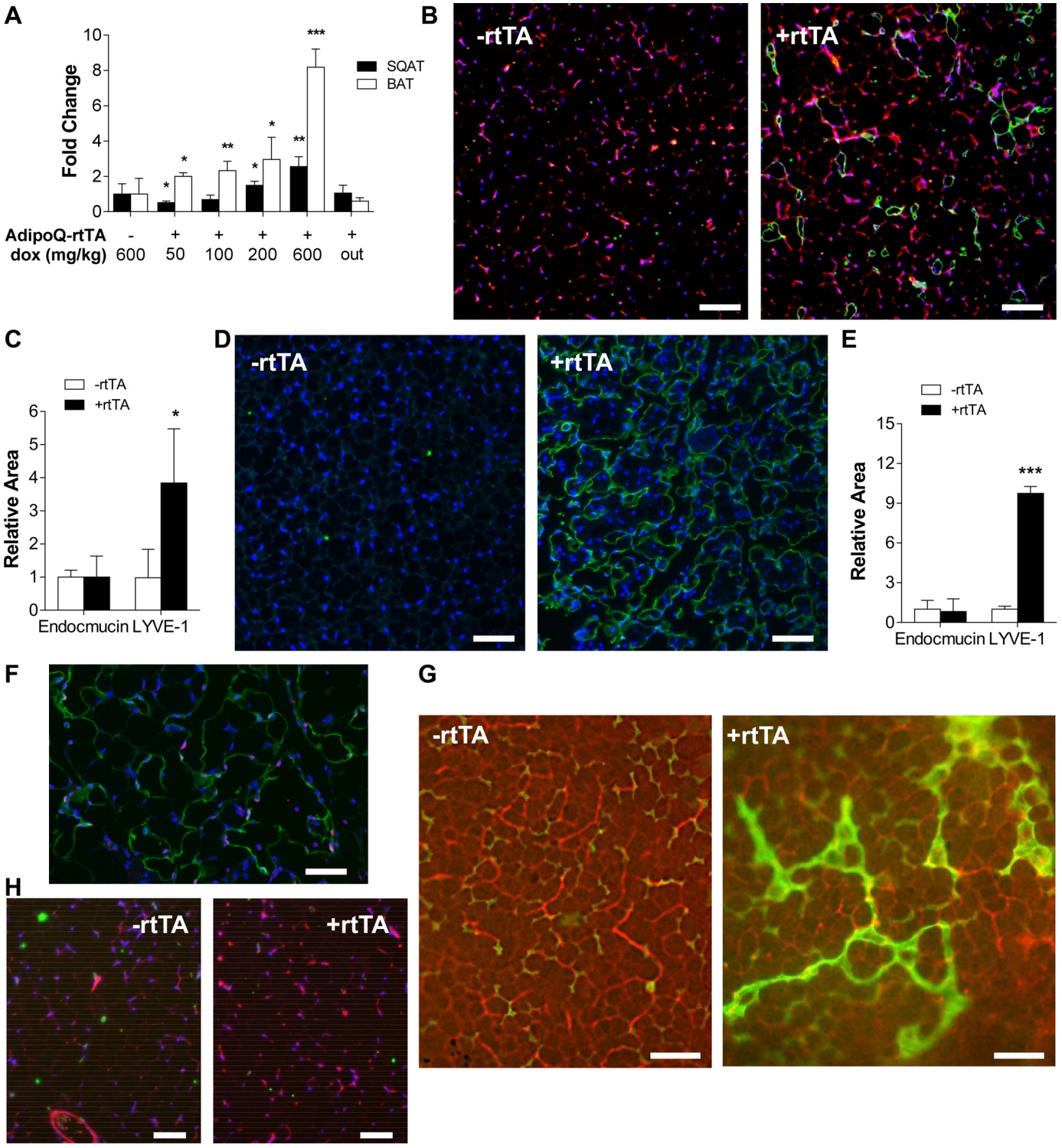

Fig. 4. Dose-dependent VEGF-D expression and lymphangiogenesis in adipose tissue of Adipo-VD mice. *A*: VEGF-D gene expression in the subcutaneous (SQAT; open bars) and interscapular brown adipose tissues (BAT; solid bars) in Adipo-VD mice demonstrate a doxycycline (dox) dose dependence when supplied in chow or drinking water. Removal of dox ("out") drops expression to basal levels. *B*: de novo lymphangiogenesis in the inguinal subcutaneous adipose depot of Adipo-VD mice after 2 mo of 600 mg/kg dox chow diet with no change in blood capillary density (LYVE-1, green; endomucin, red; DAPI, blue). *C*: quantitation of endomucin+ and LYVE-1+ areas (normalized to −rtTA) in subcutaneous adipose depot sections. $n = 4$ −rtTA and 5 +rtTA mice. *D*: BAT in Adipo-VD mice exhibits massive lymphatic hyperplasia (LYVE-1, green; DAPI, blue). *E*: endomucin+ and LYVE-1+ areas (normalized to −rtTA) quantified from BAT sections of $n = 4$ −rtTA and 5 +rtTA mice. Values are means ± SD. $^*P < 0.05$. $^{**}P < 0.01$. $^{***}P < 0.001$. *F*: new lymphatics are also podoplanin+ (green) and Prox1+ (red) in BAT of Adipo-VD mice (DAPI, blue). *G*: whole-mount LYVE-1 (green) immunofluorescence in BAT demonstrates the transition from small lymphatics to large hyperplastic lymphatic structures with no expansion of the blood capillaries (CD31, red). *H*: in a similar mouse transgenic approach, overexpression of VEGF-A under the adiponectin promoter only increases blood capillary (endomucin, red) density with no effect on lymphatics (LYVE-1, green; DAPI, blue). All scale bars = 100 μm.

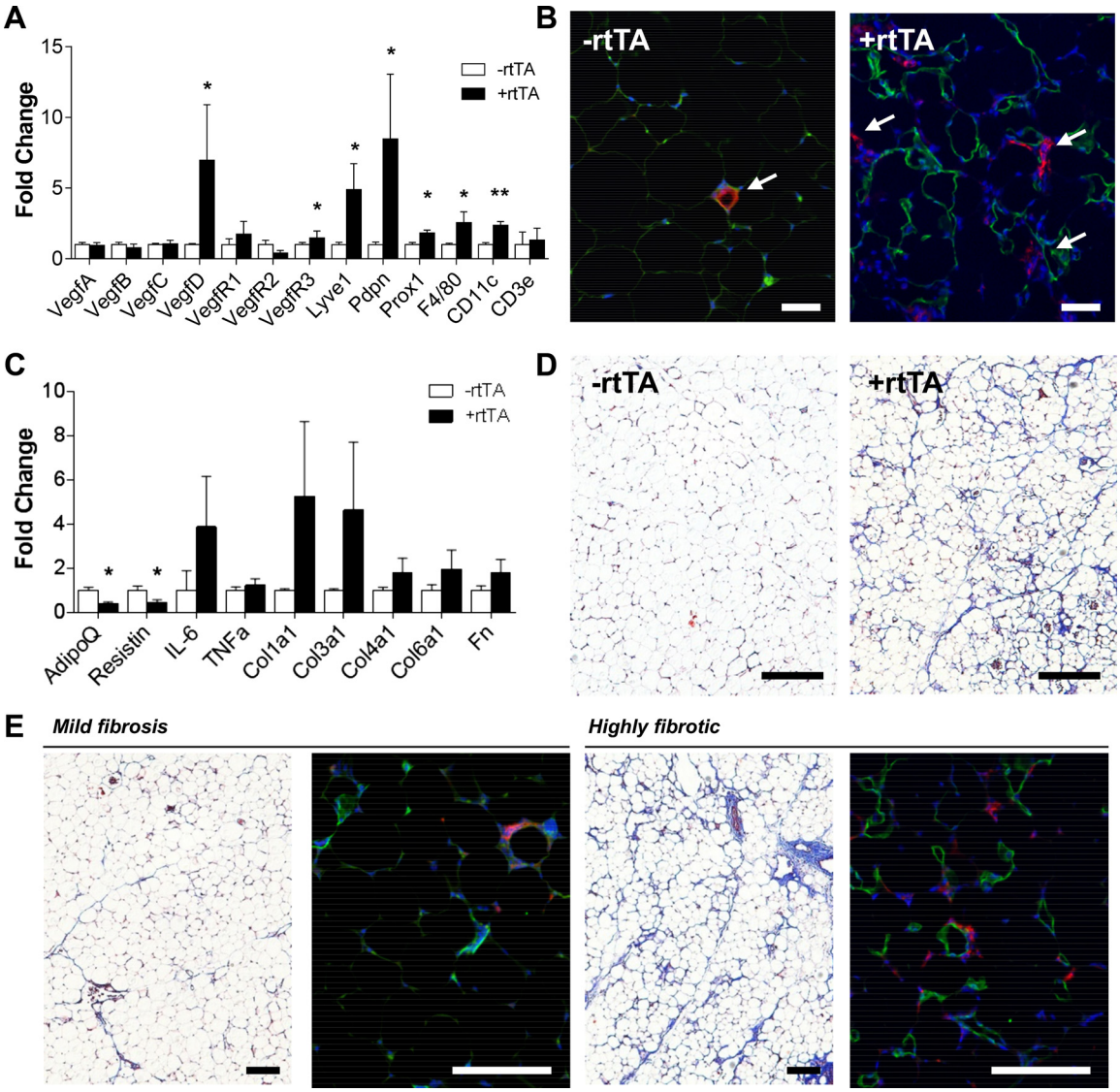

Fig. 5. Gene expression, inflammation, and fibrosis in Adipo-VD mouse white adipose tissue. *A*: quantitative RT-PCR analysis of genes in the VEGF family demonstrate only a significant increase in VEGF-D expression in inguinal subcutaneous adipose tissue. LYVE-1, VEGFR-3, podoplanin (Pdpn), and Prox1 are indicative of lymphatic endothelial cells, and macrophage markers *F4/80* and *CD11c* were also significantly elevated. *B*: Mac2 (red) immunofluorescence labels show only rare adipose crown-like structures in −rtTA tissue (arrow), but significant numbers of macrophages (arrows) in positive Adipo-VD mice near, but not colocalized with, new lymphatic structures (LYVE-1, green; DAPI, blue). Scale bars = 50 μm. *C*: white adipocyte genes for adiponectin and resistin were significantly reduced by quantitative RT-PCR analysis in Adipo-VD white adipose tissue, while proinflammatory and profibrotic matrix collagens and fibronectin gene expression tended to increase. Values are means ± SD; $n = 4$ −rtTA and 5 +rtTA mice. *$P < 0.05$. **$P < 0.01$. *D*: trichrome staining of white adipose tissue shows marked fibrosis in positive Adipo-VD mice. Scale bars = 200 μm. *E*: in Adipo-VD subcutaneous adipose tissues, the relative density of trichrome staining was proportional to the appearance of Mac2+ macrophage (red) labeling in serial sections (LYVE-1, green; DAPI, blue). Scale bars = 100 μm.

driven rtTA expression and generated a new TRE-VEGF-D mouse. In the lung and kidney, VEGF-D induces massive lymphatic hyperplasia of the existing lymphatic vessels. In the Adipo-VD mouse, prolonged VEGF-D overexpression induced de novo lymphangiogenesis, the appearance of new lymphatic vessel structures, in SQAT and hyperplasia in BAT. Interestingly, removal of the excess VEGFR-3 signaling resulted in adipose lymphatic vessel regression. In all models, the tissue's blood vascular density remained normal. We have, therefore, demonstrated this model's utility in inducing lymphatic-specific hyperplasia in several organs.

The cell source of lymphatics in development and injury has recently become a source of debate (22, 26, 29, 43); the presence or ability of "different" LECs to participate in VEGF-D-mediated lymphangiogenesis is also, therefore, likely to be tissue dependent. Rapid lymphangiectasia of the collecting vessels in the lung and kidney would suggest the response to be from the existing endothelium. In adipose tissue, the appearance of de novo lymphatic structures requires at least 1 mo (we assessed at 10 days and 2 mo) and suggests a lymphvasculogenesis or lymphagioblast-like mechanism, as has been previously reported in other systems examining postnatal and adult lymphatic expansion and regrowth (17, 21, 26, 36, 45). A return to basal VEGF-D expression resulted in a regression of the new lymphatic structures in adipose tissue, similar to the regression observed in the skin and cornea during the resolu-

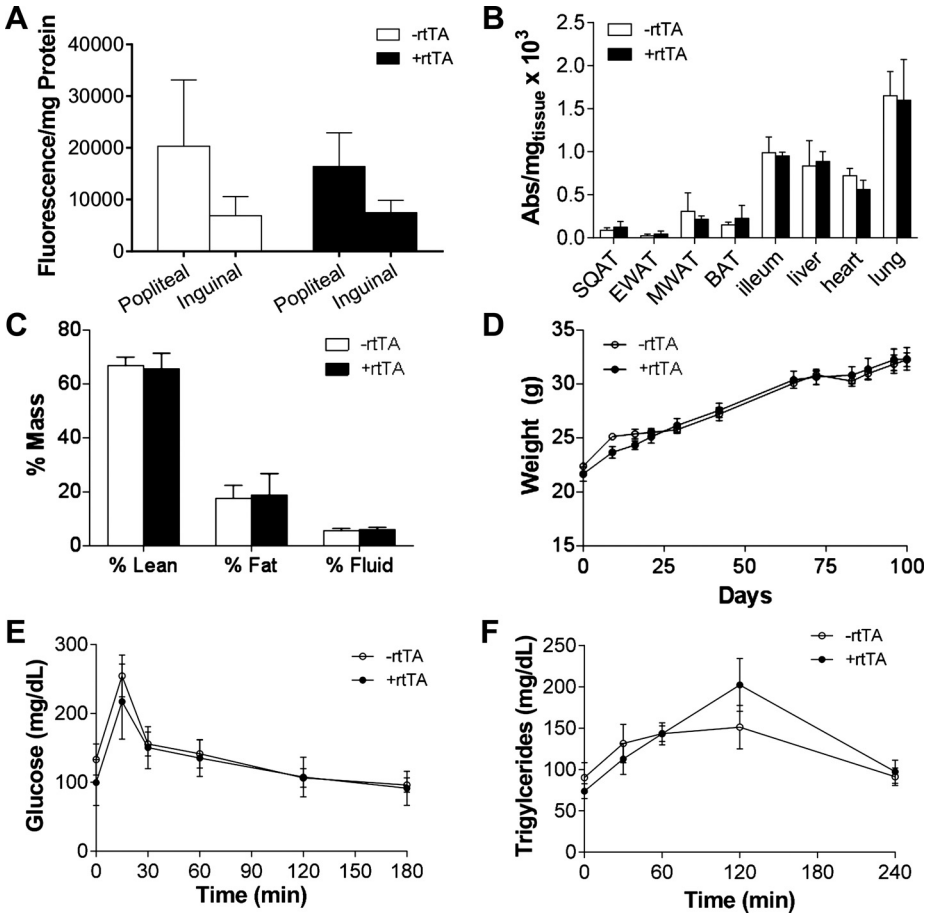

Fig. 6. Measured systemic effects of prolonged adipose tissue VEGF-D overexpression effects beyond adipose tissue depots. *A*: no change in peripheral lymphatic transport, measured by fluorescent dextran uptake to draining lymph nodes in series was measured in Adipo-VD mice. *B*: Evans blue levels in a variety of white adipose tissues depots [subcutaneous inguinal adipose tissue (SQAT); visceral epididymal adipose (EWAT); mesenteric adipose tissue (MWAT)], brown adipose tissue (BAT), and other organs were no different in positive Adipo-VD mice 30 min following intravenous injection. *C*: no changes in body composition were measured in Adipo-VD mice. *D*: weight gain on 600 mg/kg doxycycline chow was unchanged through 100 days of feeding and VEGF-D induction. *E*: Adipo-VD mice displayed normal clearance of glucose following an oral glucose challenge. *F*: oral triglyceride uptake and clearance were unchanged in Adipo-VD mice. Values are means ± SD; $n = 4$ −rtTA and 5 +rtTA mice (*A*); $n = 3$ −rtTA and 4 +rtTA mice (*B*); $n = 4$ −rtTA and 6 +rtTA mice (*C–F*).

tion of inflammation (10, 19, 28). While this is not surprising, given the transient nature of the hyperplasic signal in this model, in the adult intestine, continued VEGFR-3 signaling via VEGF-C was absolutely necessary to maintain even the normal adult lymphatic vasculature in an elegant study utilizing an adult model of inducible systemic VEGF-C deletion (30). This regression is in contrast to models of airway lymphatic hyperplasia, induced by either inflammation or VEGF-C/D expression methods, which exists even once the driver is removed (7, 54). The ability to grow lymphatic vessels, the mechanism by which expansion occurs, and the potential for regression thus appear to be varying degrees of VEGFR-3, developmental period, and tissue dependent (3, 25). The TRE-VD mouse, coupled with the array of cell-specific promoter mice available, allows for a future temporal examination of these mechanisms in nearly any vascularized tissue.

Lymphatic expansion is characteristic in inflammatory models with an upregulation of lymphangiogenic factors in the tissue (7, 38, 55). Some level of VEGFR-3 signaling and lymphangiogenesis, however, appears to be necessary to reduce inflammation under challenge (3, 48). The role of lymphatics in regulating tissue inflammation is highly relevant to the global obesity epidemic, wherein adipose tissue inflammation, notably infiltrating immune cells, are thought to drive the metabolic syndrome (1, 33, 52). The interaction of lymphatic vessels with surrounding adipose tissue is thus of paramount interest. Defective lymphatic function, or lymph "leaking" from the lymphatic vasculature, has been demonstrated to be pro-adipogenic, leading to local and systemic depot expansion, and hence may play a role in obesity and the metabolic syndrome (2, 16, 23, 38, 56). A recent study by Karaman and colleagues (20) clearly demonstrated that VEGFR-3 signaling was partially responsible for the recruitment of proinflammatory macrophages to adipose tissue in diet-induced obesity; blockade of these cells improved the metabolic phenotype. The Adipo-VD model exhibited not only increased macrophage infiltration, but also fibrosis. What role macrophages play in the fibrosis directly or in the mechanisms of adipose tissue lymphangiogenesis remains to be examined. It is also possible that the increased lymphatic vasculature provides a route for the cells, or that it is locally dysfunctional and involved in the inflammatory and fibrotic process; again, this remains to be tested. It is noteworthy that the apparent inflammation in white adipose tissue did not result in a blatant insulin-insensitive phenotype. The ability of adipocytes to safely partition excessive dietary lipid protects from the metabolic syndrome rather than adipose macrophages directly (44, 49). How increased lymphatic vascularization may impact other adipose tissue functions, and its impact in obesity, will be an interesting application of this inducible VEGF-D model in understanding metabolic and adipose tissues pathologies.

VEGFR-3 signaling may not only induce hyperplasia, but also impact lymphatic vessel fluid and cell transport in a host of tissue systems (8, 14, 15, 41, 42). The Adipo-VD mouse did not display systemic edema, assessed by total body fluid accumulation. However, the quality of local lymphatic function

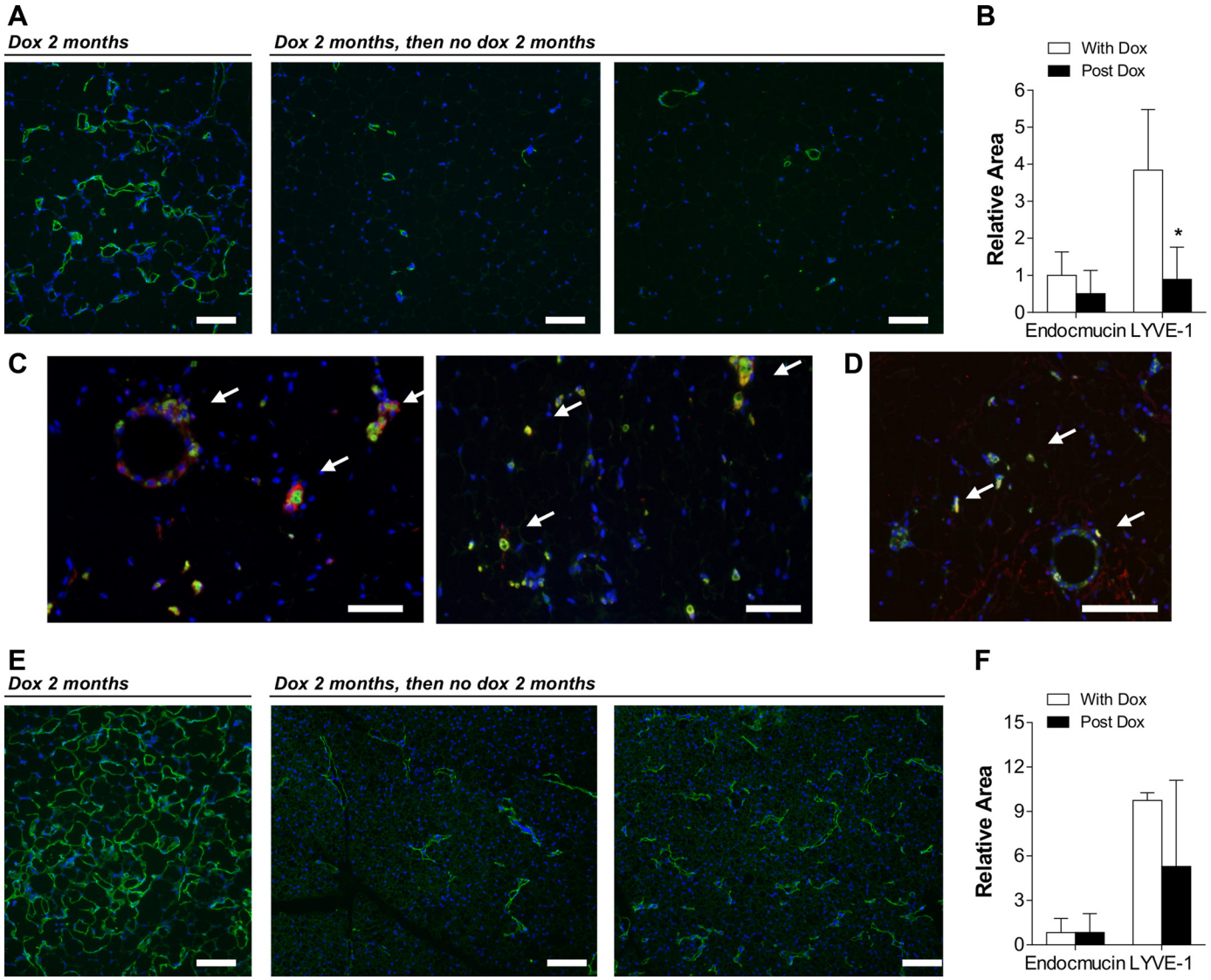

Fig. 7. Regression of adipose tissue and the newly formed adipose tissue lymphatics following removal of doxycycline (dox). *A*: the extensive lymphatic expansion in subcutaneous adipose tissue following 2 mo of 600 mg/kg dox diet (LYVE-1, *left*) regresses if mice are returned to standard chow diet for 2 mo (*right*; imaged from 2 mice). Few lymphatic vessel structures are found in subcutaneous white adipose tissue once VEGF-D is no longer overexpressed (DAPI, blue). *B*: quantitation of endomucin+ and LYVE-1+ areas demonstrating reduced lymphatic density. $n = 4$ mice each. *C*: LYVE-1+ cells localize with newly forming crown-like structures (Mac2, red; arrows) in white adipose tissue or appear as single cells (arrows) after 2 mo of regression in two different mice (DAPI; blue). *D*: podoplanin+ cells (green) also incorporate and colocalize with Mac2+ macrophage labeling (red) in cells and crown-like structures (arrows; DAPI, blue). *E*: in brown adipose tissue of Adipo-VD mice, the massive lymphatic hypertrophy after VEGF-D overexpression (*left*; LYVE-1, green) regresses with removal of dox chow (*right*; imaged from 2 mice), but numerous large LYVE-1+ structures still remain (DAPI, blue). All scale bars = 100 μm. *F*: quantitation of endomucin+ and LYVE-1+ areas highlights the variability in lymphatic regression in brown adipose. Values are means ± SE; $n = 8$ mice each. $^*P < 0.05$.

to clear interstitial fluid or traffic immune cells from the hyperplastic areas or the impact of excess VEGF-D on collecting lymphatic vessel contractility was not directly tested. Assessment of blood capillary effects by Evans blue flux alone may not fully reveal changes in fluid flux (e.g., increased extravasation, but also increased lymphatic uptake, resulting in no net difference in Adipo-VD mice). Whether lower levels of dox, and thus lower levels of excess VEGF-D (that did not lead to pathological lymphangiogenesis in the tissues tested) do not still impact lymphatic function is unknown. A bigger question may be why the lymphangiogenic effects were so digitized at a specific dox/VEGF-D level: an answer to which will have to be determined through a careful dose and temporal time course in each tissue model. The limitations of the TRE-VD model may be that its signaling impact on large vessels precludes the ability to grow new lymphatic vasculature in a tissue, as seen in the KSP-VD model. Similarly, any benefits of an increased lymphatic vasculature may be offset by the proinflammatory effect of VEGF-D, typical problems in characterizing any transgenic approach.

In summary, we have developed a novel mouse model of inducible murine VEGF-D overexpression that has demonstrated utility in multiple organ systems to drive lymphatic hyperplasia. In adipose tissue in particular, the ability of VEGF-D signaling through VEGFR-3 is sufficient to induce de novo lymphangiogenesis and a vasculature that regresses upon

removal of the signal. This highlights the utility of this specific TRE-VD platform for further studies of the roles of lymphatic transport, LEC biology, and the development and maintenance of lymphatic vasculature in health and disease.

ACKNOWLEDGMENTS

The authors thank Philipp Scherer and the Touchstone Diabetes Center for the *AdipoQ*-rtTA mouse and the George M. O'Brien Kidney Core Center at UT Southwestern Medical Center for the *KSP*-rtTA mouse. We also thank Qiong A. Wang and Kai Sun of the Touchstone Diabetes Center for assistance in TRE-VEGF-D vector design and construction, and Nynke van Polanen for animal help and technical assistance.

GRANTS

J. M. Rutkowski was supported by the American Heart Association (12SDG12050287) and the Texas A&M Health Science Center College of Medicine.

DISCLOSURES

No conflicts of interest, financial or otherwise, are declared by the author(s).

AUTHOR CONTRIBUTIONS

G.M.L., C.E.V.Z., D.X.G., J.L.O., M.T.D., and J.M.R. performed experiments; G.M.L., C.E.V.Z., D.X.G., J.L.O., M.T.D., and J.M.R. analyzed data; G.M.L., C.E.V.Z., D.X.G., J.L.O., M.T.D., and J.M.R. interpreted results of experiments; G.M.L., C.E.V.Z., D.X.G., M.T.D., and J.M.R. edited and revised manuscript; G.M.L., C.E.V.Z., D.X.G., J.L.O., M.T.D., and J.M.R. approved final version of manuscript; J.M.R. conception and design of research; J.M.R. prepared figures; J.M.R. drafted manuscript.

REFERENCES

1. **Aouadi M, Tencerova M, Vangala P, Yawe JC, Nicoloro SM, Amano SU, Cohen JL, Czech MP.** Gene silencing in adipose tissue macrophages regulates whole-body metabolism in obese mice. *Proc Natl Acad Sci U S A* 110: 8278–8283, 2013.
2. **Aschen S, Zampell JC, Elhadad S, Weitman E, De Brot M, Mehrara BJ.** Regulation of adipogenesis by lymphatic fluid stasis. II. Expression of adipose differentiation genes. *Plast Reconstr Surg* 129: 838–847, 2012.
3. **Aspelund A, Robciuc MR, Karaman S, Makinen T, Alitalo K.** Lymphatic system in cardiovascular medicine. *Circ Res* 118: 515–530, 2016.
4. **Baldwin ME, Catimel B, Nice EC, Roufail S, Hall NE, Stenvers KL, Karkkainen MJ, Alitalo K, Stacker SA, Achen MG.** The specificity of receptor binding by vascular endothelial growth factor-d is different in mouse and man. *J Biol Chem* 276: 19166–19171, 2001.
5. **Baldwin ME, Roufail S, Halford MM, Alitalo K, Stacker SA, Achen MG.** Multiple forms of mouse vascular endothelial growth factor-D are generated by RNA splicing and proteolysis. *J Biol Chem* 276: 44307–44314, 2001.
6. **Baluk P, Hogmalm A, Bry M, Alitalo K, Bry K, McDonald DM.** Transgenic overexpression of interleukin-1beta induces persistent lymphangiogenesis but not angiogenesis in mouse airways. *Am J Pathol* 182: 1434–1447, 2013.
7. **Baluk P, Tammela T, Ator E, Lyubynska N, Achen MG, Hicklin DJ, Jeltsch M, Petrova TV, Pytowski B, Stacker SA, Yla-Herttuala S, Jackson DG, Alitalo K, McDonald DM.** Pathogenesis of persistent lymphatic vessel hyperplasia in chronic airway inflammation. *J Clin Invest* 115: 247–257, 2005.
8. **Breslin JW, Gaudreault N, Watson KD, Reynoso R, Yuan SY, Wu MH.** Vascular endothelial growth factor-C stimulates the lymphatic pump by a VEGF receptor-3-dependent mechanism. *Am J Physiol Heart Circ Physiol* 293: H709–H718, 2007.
9. **Cao R, Eriksson A, Kubo H, Alitalo K, Cao Y, Thyberg J.** Comparative evaluation of FGF-2-, VEGF-A-, and VEGF-C-induced angiogenesis, lymphangiogenesis, vascular fenestrations, and permeability. *Circ Res* 94: 664–670, 2004.
10. **Cursiefen C, Maruyama K, Jackson DG, Streilein JW, Kruse FE.** Time course of angiogenesis and lymphangiogenesis after brief corneal inflammation. *Cornea* 25: 443–447, 2006.
11. **Dixelius J, Makinen T, Wirzenius M, Karkkainen MJ, Wernstedt C, Alitalo K, Claesson-Welsh L.** Ligand-induced vascular endothelial growth factor receptor-3 (VEGFR-3) heterodimerization with VEGFR-2 in primary lymphatic endothelial cells regulates tyrosine phosphorylation sites. *J Biol Chem* 278: 40973–40979, 2003.
12. **Dixon JB.** Lymphatic lipid transport: sewer or subway? *Trends Endocrinol Metab* 21: 480–487, 2010.
13. **Gashev AA, Chatterjee V.** Aged lymphatic contractility: recent answers and new questions. *Lymphat Res Biol* 11: 2–13, 2013.
14. **Gogineni A, Caunt M, Crow A, Lee CV, Fuh G, van Bruggen N, Ye W, Weimer RM.** Inhibition of VEGF-C modulates distal lymphatic remodeling and secondary metastasis. *PloS One* 8: e68755, 2013.
15. **Goldman J, Le TX, Skobe M, Swartz MA.** Overexpression of VEGF-C causes transient lymphatic hyperplasia but not increased lymphangiogenesis in regenerating skin. *Circ Res* 96: 1193–1199, 2005.
16. **Harvey NL, Srinivasan RS, Dillard ME, Johnson NC, Witte MH, Boyd K, Sleeman MW, Oliver G.** Lymphatic vascular defects promoted by Prox1 haploinsufficiency cause adult-onset obesity. *Nat Genet* 37: 1072–1081, 2005.
17. **Hogan BM, Bos FL, Bussmann J, Witte M, Chi NC, Duckers HJ, Schulte-Merker S.** Ccbe1 is required for embryonic lymphangiogenesis and venous sprouting. *Nat Genet* 41: 396–398, 2009.
18. **Jeltsch M, Kaipainen A, Joukov V, Meng X, Lakso M, Rauvala H, Swartz M, Fukumura D, Jain RK, Alitalo K.** Hyperplasia of lymphatic vessels in VEGF-C transgenic mice. *Science* 276: 1423–1425, 1997.
19. **Kang GJ, Ecoiffier T, Truong T, Yuen D, Li G, Lee N, Zhang L, Chen L.** Intravital imaging reveals dynamics of lymphangiogenesis and valvulogenesis. *Sci Rep* 6: 19459, 2016.
20. **Karaman S, Hollmen M, Robciuc MR, Alitalo A, Nurmi H, Morf B, Buschle D, Alkan HF, Ochsenbein AM, Alitalo K, Wolfrum C, Detmar M.** Blockade of VEGF-C and VEGF-D modulates adipose tissue inflammation and improves metabolic parameters under high-fat diet. *Mol Metab* 4: 93–105, 2015.
21. **Kelly-Goss MR, Sweat RS, Azimi MS, Murfee WL.** Vascular islands during microvascular regression and regrowth in adult networks. *Front Physiol* 4: 108, 2013.
22. **Klotz L, Norman S, Vieira JM, Masters M, Rohling M, Dube KN, Bollini S, Matsuzaki F, Carr CA, Riley PR.** Cardiac lymphatics are heterogeneous in origin and respond to injury. *Nature* 522: 62–67, 2015.
23. **Kuan EL, Ivanov S, Bridenbaugh EA, Victora G, Wang W, Childs EW, Platt AM, Jakubzick CV, Mason RJ, Gashev AA, Nussenzweig M, Swartz MA, Dustin ML, Zawieja DC, Randolph GJ.** Collecting lymphatic vessel permeability facilitates adipose tissue inflammation and distribution of antigen to lymph node-homing adipose tissue dendritic cells. *J Immunol* 194: 5200–5210, 2015.
24. **Lim HY, Rutkowski JM, Helft J, Reddy ST, Swartz MA, Randolph GJ, Angeli V.** Hypercholesterolemic mice exhibit lymphatic vessel dysfunction and degeneration. *Am J Pathol* 175: 1328–1337, 2009.
25. **Makinen T, Jussila L, Veikkola T, Karpanen T, Kettunen MI, Pulkkanen KJ, Kauppinen R, Jackson DG, Kubo H, Nishikawa S, Yla-Herttuala S, Alitalo K.** Inhibition of lymphangiogenesis with resulting lymphedema in transgenic mice expressing soluble VEGF receptor-3. *Nat Med* 7: 199–205, 2001.
26. **Martinez-Corral I, Ulvmar MH, Stanczuk L, Tatin F, Kizhatil K, John SW, Alitalo K, Ortega S, Makinen T.** Nonvenous origin of dermal lymphatic vasculature. *Circ Res* 116: 1649–1654, 2015.
27. **Miller NE, Michel CC, Nanjee MN, Olszewski WL, Miller IP, Hazell M, Olivecrona G, Sutton P, Humphreys SM, Frayn KN.** Secretion of adipokines by human adipose tissue in vivo: partitioning between capillary and lymphatic transport. *Am J Physiol Endocrinol Metab* 301: E659–E667, 2011.
28. **Mumprecht V, Roudnicky F, Detmar M.** Inflammation-induced lymph node lymphangiogenesis is reversible. *Am J Pathol* 180: 874–879, 2012.
29. **Nicenboim J, Malkinson G, Lupo T, Asaf L, Sela Y, Mayseless O, Gibbs-Bar L, Senderovich N, Hashimshony T, Shin M, Jerafi-Vider A, Avraham-Davidi I, Krupalnik V, Hofi R, Almog G, Astin JW, Golani O, Ben-Dor S, Crosier PS, Herzog W, Lawson ND, Hanna JH, Yanai I, Yaniv K.** Lymphatic vessels arise from specialized angioblasts within a venous niche. *Nature* 522: 56–61, 2015.
30. **Nurmi H, Saharinen P, Zarkada G, Zheng W, Robciuc MR, Alitalo K.** VEGF-C is required for intestinal lymphatic vessel maintenance and lipid absorption. *EMBO Mol Med* 7: 1418–1425, 2015.
31. **Pan X, Small EV, Igarashi P, Carroll TJ.** Generation and characterization of KsprtTA and KsptTA transgenic mice. *Genesis* 51: 430–435, 2013.
32. **Paquet-Fifield S, Levy SM, Sato T, Shayan R, Karnezis T, Davydova N, Nowell CJ, Roufail S, Ma GZ, Zhang YF, Stacker SA, Achen MG.**

Vascular endothelial growth factor-d modulates caliber and function of initial lymphatics in the dermis. *J Invest Dermatol* 133: 2074–2084, 2013.
33. **Patsouris D, Li PP, Thapar D, Chapman J, Olefsky JM, Neels JG.** Ablation of CD11c-positive cells normalizes insulin sensitivity in obese insulin resistant animals. *Cell Metab* 8: 301–309, 2008.
34. **Randolph GJ, Miller NE.** Lymphatic transport of high-density lipoproteins and chylomicrons. *J Clin Invest* 124: 929–935, 2014.
35. **Rockson SG.** Laboratory models for the investigation of lymphangiomatosis. *Microvasc Res* 96: 64–67, 2014.
36. **Rutkowski JM, Boardman KC, Swartz MA.** Characterization of lymphangiogenesis in a model of adult skin regeneration. *Am J Physiol Heart Circ Physiol* 291: H1402–H1410, 2006.
37. **Rutkowski JM, Davis KE, Scherer PE.** Mechanisms of obesity and related pathologies: the macro- and microcirculation of adipose tissue. *FEBS J* 276: 5738–5746, 2009.
38. **Rutkowski JM, Moya M, Johannes J, Goldman J, Swartz MA.** Secondary lymphedema in the mouse tail: lymphatic hyperplasia, VEGF-C upregulation, and the protective role of MMP-9. *Microvasc Res* 72: 161–171, 2006.
39. **Rutkowski JM, Stern JH, Scherer PE.** The cell biology of fat expansion. *J Cell Biol* 208: 501–512, 2015.
40. **Saaristo A, Veikkola T, Enholm B, Hytonen M, Arola J, Pajusola K, Turunen P, Jeltsch M, Karkkainen MJ, Kerjaschki D, Bueler H, Yla-Herttuala S, Alitalo K.** Adenoviral VEGF-C overexpression induces blood vessel enlargement, tortuosity, and leakiness but no sprouting angiogenesis in the skin or mucous membranes. *FASEB J* 16: 1041–1049, 2002.
41. **Savetsky IL, Albano NJ, Cuzzone DA, Gardenier JC, Torrisi JS, Garcia Nores GD, Nitti MD, Hespe GE, Nelson TS, Kataru RP, Dixon JB, Mehrara BJ.** Lymphatic function regulates contact hypersensitivity dermatitis in obesity. *J Invest Dermatol* 135: 2742–2752, 2015.
42. **Sevick-Muraca EM, King PD.** Lymphatic vessel abnormalities arising from disorders of Ras signal transduction. *Trends Cardiovasc Med* 24: 121–127, 2014.
43. **Stanczuk L, Martinez-Corral I, Ulvmar MH, Zhang Y, Lavina B, Fruttiger M, Adams RH, Saur D, Betsholtz C, Ortega S, Alitalo K, Graupera M, Makinen T.** cKit lineage hemogenic endothelium-derived cells contribute to mesenteric lymphatic vessels. *Cell Rep* 10: 1708–1721, 2015.
44. **Stern JH, Rutkowski JM, Scherer PE.** Adiponectin, leptin, and fatty acids in the maintenance of metabolic homeostasis through adipose tissue crosstalk. *Cell Metab* 23: 770–784, 2016.
45. **Stoll SJ, Bartsch S, Kroll J.** HOXC9 regulates formation of parachordal lymphangioplasts and the thoracic duct in zebrafish via stabilin 2. *PloS One* 8: e58311, 2013.
46. **Sun K, Wernstedt Asterholm I, Kusminski CM, Bueno AC, Wang ZV, Pollard JW, Brekken RA, Scherer PE.** Dichotomous effects of VEGF-A on adipose tissue dysfunction. *Proc Natl Acad Sci U S A* 109: 5874–5879, 2012.
47. **Tammela T, Enholm B, Alitalo K, Paavonen K.** The biology of vascular endothelial growth factors. *Cardiovasc Res* 65: 550–563, 2005.
48. **Thomas SN, Rutkowski JM, Pasquier M, Kuan EL, Alitalo K, Randolph GJ, Swartz MA.** Impaired humoral immunity and tolerance in K14-VEGFR-3-Ig mice that lack dermal lymphatic drainage. *J Immunol* 189: 2181–2190, 2012.
49. **Unger RH, Scherer PE.** Gluttony, sloth and the metabolic syndrome: a roadmap to lipotoxicity. *Trends Endocrinol Metab* 21: 345–352, 2010.
50. **Vuorio T, Nurmi H, Moulton K, Kurkipuro J, Robciuc MR, Ohman M, Heinonen SE, Samaranayake H, Heikura T, Alitalo K, Yla-Herttuala S.** Lymphatic vessel insufficiency in hypercholesterolemic mice alters lipoprotein levels and promotes atherogenesis. *Arterioscler Thromb Vasc Biol* 34: 1162–1170, 2014.
51. **Wang ZV, Deng Y, Wang QA, Sun K, Scherer PE.** Identification and characterization of a promoter cassette conferring adipocyte-specific gene expression. *Endocrinology* 151: 2933–2939, 2010.
52. **Wernstedt Asterholm I, Tao C, Morley TS, Wang QA, Delgado-Lopez F, Wang ZV, Scherer PE.** Adipocyte inflammation is essential for healthy adipose tissue expansion and remodeling. *Cell Metab* 20: 103–118, 2014.
53. **Xu KF, Zhang P, Tian X, Ma A, Li X, Zhou J, Zeng N, Gui YS, Guo Z, Feng R, Zhang W, Sun W, Cai B.** The role of vascular endothelial growth factor-D in diagnosis of lymphangioleiomyomatosis (LAM). *Respir Med* 107: 263–268, 2013.
54. **Yao LC, Testini C, Tvorogov D, Anisimov A, Vargas SO, Baluk P, Pytowski B, Claesson-Welsh L, Alitalo K, McDonald DM.** Pulmonary lymphangiectasia resulting from vascular endothelial growth factor-C overexpression during a critical period. *Circ Res* 114: 806–822, 2014.
55. **Yazdani S, Navis G, Hillebrands JL, van Goor H, van den Born J.** Lymphangiogenesis in renal diseases: passive bystander or active participant? *Expert Rev Mol Med* 16: e15, 2014.
56. **Zampell JC, Aschen S, Weitman ES, Yan A, Elhadad S, De Brot M, Mehrara BJ.** Regulation of adipogenesis by lymphatic fluid stasis: part I. Adipogenesis, fibrosis, and inflammation. *Plast Reconstr Surg* 129: 825–834, 2012.
57. **Zheng W, Aspelund A, Alitalo K.** Lymphangiogenic factors, mechanisms, applications. *J Clin Invest* 124: 878–887, 2014.